Infrared and Raman spectra and lattice dynamics of the superionic conductor Li_3N

H. R. Chandrasekhar,* G. Bhattacharya, R. Migoni, and H. Bilz
Max-Planck-Institut für Festkörperforschung, 7 Stuttgart-80, Federal Republic of Germany
(Received 31 May 1977)

The polarized infrared and Raman spectra of hexagonal Li_3N (space group D_{6h}^1) are reported. The frequencies of the infrared-active phonons and the dielectric constants are determined from a Kramers-Kronig analysis and oscillator fits to the reflectivity data. A group-theoretical analysis has permitted an identification of the symmetries of the infrared- and Raman-active phonons. The frequencies of these phonons are used to determine the parameters of a rigid-shell model which includes the anisotropic polarizability of the nitrogen ions. The calculated dispersion curves are discussed in connection with the second-order Raman spectra. It is concluded that Li_3N is the first known compound in which the nitrogen ions are close to an anomalous N^{3-} state.

I. INTRODUCTION

Recently there has been a considerable interest in the static and dynamic properties of lithium nitride, Li_3N. This material exhibits a large ionic conductivity comparable to that of Li β-alumina, pointing to important applications as a lithium-conducting solid electrolyte.[1,2] Lithium is specially suited for applications in energy-storage devices due to its low equivalent weight and strong electropositive character. The only (other) lithium compound with an ionic conductivity comparable to that of Na β-alumina is Li β-alumina. However, unlike lithium nitride, Li β-alumina is thermodynamically unstable at elevated temperatures with respect to lithium, thus restricting its applications.[3,4] Another interesting aspect of Li_3N is that it is the first compound known to have nitrogen ions in an anomalous N^{3-} state as will be shown in this paper. It is well known that the large and nonlinear polarizability of the O^{2-} ion, which arises from its instability as a free ion, plays a very important role in the dynamical properties of oxides such as MgO and $SrTiO_3$.[5] On the other hand, the N^{3-} ion should be even more unstable. Hence it is to be expected that its polarizability should play a significant role in determining the phonon dispersion relations and the Raman spectra of Li_3N. The superionic conductivity of this material might also be related to the nitrogen polarizability. Therefore, Li_3N serves as an important model substance. It will be shown in this paper and a later publication[6] that, indeed, the intraionic polarizability of N^{3-}, in particular its anisotropy, is crucial in the understanding of various dynamical properties of Li_3N.

The crystal structure of Li_3N has been shown to be hexagonal with four atoms per unit cell.[7,8] The unit-cell dimensions are $a = 3.648$ Å and $c = 3.875$ Å. The symmetry point group is D_{6h} (space group $P6/mmm$). The structure is typically ionic with the N^{3-} coordinated in a regular way with eight Li^+ ions. As shown in Fig. 1, the structure can be visualized to consist of Li_2N layers normal to the z axis connected by one lithium atom per unit cell which occupies a site in the middle of the layers. In a layer each N and Li atom form six and three bonds, respectively, whereas only two N-Li bonds are responsible for the connection of the layers.[8] We have defined the axes x and y in the hexagonal plane as shown in Fig. 1. The Cartesian coordinates of the ions in the unit cell are $(0,0,0)$ for nitrogen, and $\frac{1}{2}a, \frac{1}{2}a/\sqrt{3}, 0)$, $(\frac{1}{2}a, -\frac{1}{2}a/\sqrt{3}, 0)$, and $(0, 0, \frac{1}{2}c)$ for lithium.

In this paper we present polarized-infrared-reflectivity and Raman spectra for oriented single crystals of Li_3N. The values of zone-center optical-phonon frequencies and dielectric constants are determined. A factor group analysis is performed and the symmetries of observed phonons are identified. A rigid-shell model with eight parameters, which includes the nearest-neighbor interactions only and the anisotropic polarizability of the nitrogen ion, yields an excellent fit to the

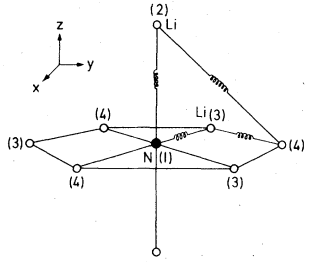

FIG. 1. Crystal structure of Li_3N. The eightfold coordination of N^{3-} and Li^+ ions is shown. The solid points and open circles represent nitrogen and lithium, respectively. The Li(2) occupies a site in the middle of layers along the z axis. The y axis is defined to be along the line connecting N(1) and Li(4).

zone-center phonon frequencies. The complete phonon dispersion curves are obtained and discussed in connection with the second-order Raman spectra. Preliminary results have been published elsewhere.[9]

II. EXPERIMENT

A. Samples

The single crystals of Li_3N were grown by the Czochralski method[8] and oriented from conventional Laue photographs. The samples were cut using a precision diamond-impregnated annular saw for measurements on the face containing or normal to the z axis. The samples were carefully lapped and gently polished using suspensions of alumina abrasive in paraffin oil on polishing cloths. The final polishing was done with tiny amounts of methanol instead of the paraffin oil. Due to the hygroscopic nature of the samples, it was necessary to preserve the samples in vacuum desiccators. The Raman measurements were done with the sample in evacuated cryostats. The infrared measurements were performed by drying or evacuating the sample chamber in the spectrometers. A final polish immediately prior to measurement was found to be necessary in spite of the precautions taken to preserve the samples.

B. Infrared reflectivity measurements

Figures 2 and 3 show the results of infrared reflectivity measurements at 300 °K. A Polytec FIR 30 Fourier spectrometer and a Perkin Elmer Model 180 grating spectrophotometer were used. A wire-grid polarizer which could be rotated by 90° was used for recording the polarized spectra. The spectrum for $\vec{E} \perp \vec{z}$ in Fig. 2 was measured on an

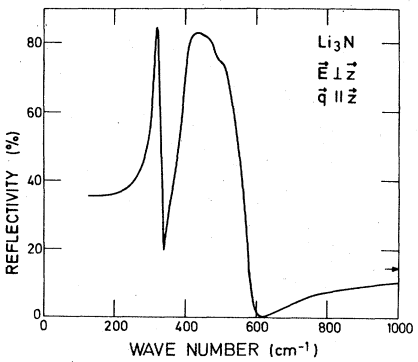

FIG. 2. Room-temperature reflectivity spectrum of Li_3N measured on the hexagonal plane for the electric vector E perpendicular to the z axis. The arrow on the right-hand side indicates the value of reflectivity measured at 4000 cm^{-1}.

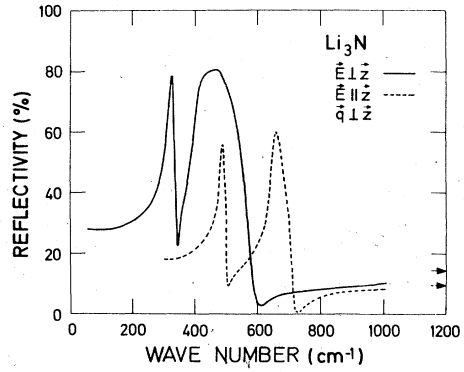

FIG. 3. Room-temperature reflectivity spectra of Li_3N measured on a face containing the z axis for E parallel and perpendicular to z. The arrows on the right-hand side indicate the values of reflectivity measured at 4000 cm^{-1}.

oriented z face. The spectrum on the z face showed no polarization dependence and was identical to Fig. 2 when the polarization was rotated in the z plane. The spectra for $\vec{E} \perp \vec{z}$ and $\vec{E} \parallel \vec{z}$ in Fig. 3 were recorded on a face containing the z axis. These spectra show pronounced polarization dependence. The crystal had to be carefully oriented with respect to the electric field, particularly for measurements with $\vec{E} \parallel \vec{z}$, in order to avoid any leakage of the strong $\vec{E} \perp \vec{z}$ spectrum. The spectra for $\vec{E} \perp \vec{z}$ are identical for $\vec{q} \parallel \vec{z}$ and $\vec{q} \perp \vec{z}$. The values of reflectivity, however, were somewhat lower for $\vec{q} \perp \vec{z}$ measurements due to the inferior quality of the surface compared to the z face. The reflectivity measurements were extended up to 4000 cm^{-1} ($\lambda = 2.5\ \mu m$) in order to obtain reliable values for ϵ_∞. The structureless region is not shown in Figs. 2 and 3. Instead, the reflectivity measured at 4000 cm^{-1} is indicated by an arrow at the right-hand edges of these figures.

C. Raman measurements

Raman spectra were recorded at room temperature using the back scattering configuration. A Spex Triple monochromator, equipped with photon counting electronics was used. The 6471-Å line of a Kr^+ laser was used as the excitation source. Though the sample is transparent to this radiation, it was not possible to perform right-angle scattering due to the difficulties of sample preparation. A strong first-order line was observed for (xx), (yy), and (xy); here the notation (xz) for example, indicates that x and z are the polarization vectors of the incident and scattered photons, respectively. The wave vectors of the incident and scattered light were normal to the scattering plane (see Fig. 3 of Ref. 9).

III. THEORY AND DISCUSSION

A. Symmetry analysis

The Brillouin zone (BZ) of the hexagonal lattice with D_{6h} point-group symmetry of Li_3N is shown in Fig. 4. We have studied the symmetry properties of the phonons for wave vector $\vec{q}$ along the three principal symmetry directions x, y, and z. These are the same directions as shown in Fig. 1 with reference to the direct lattice. We shall not describe in detail the well-known procedure of group-theoretical analysis[10,11] except for the following relevant points. The normal modes of vibration are classified by assigning them to the irreducible representations of the space group of the crystal, D_{6h}^1 $(P6/mmm)$. This being a symmorphic space group, its irreducible representations can be obtained from the irreducible representations of the point group $G_{\vec{q}}$ corresponding to the wave vector $\vec{q}$. The number of normal modes which correspond to a given irreducible representation j of $G_{\vec{q}}$ is given by

$$n_j(\vec{q}) = \frac{1}{N_{\vec{q}}} \sum_{R \in G_{\vec{q}}} \chi^{(j)}(R, \vec{q}) \chi(R, \vec{q}) , \qquad (1)$$

where R are the symmetry operations of $G_{\vec{q}}$ and $\chi^{(j)}(R, \vec{q})$ are their characters in the irreducible representation j. $N_{\vec{q}}$ is the order of $G_{\vec{q}}$. The character $\chi(R, \vec{q})$ of R in the twelve-dimensional reducible representation of $G_{\vec{q}}$ are calculated according to the formula

$$\chi(R, \vec{q}) = (\pm 1 + 2\cos\theta_R) N_R . \qquad (2)$$

Here N_R is the number of atoms in the unit cell which are left in the equivalent positions as a result of the operation R. The (+) and (−) signs refer to the proper and improper rotations, respectively, by the angle θ_R. For the points at the boundary of the BZ which are displaced by a reciprocal-lattice vector $\vec{G}$ under the operation R, N_R is replaced by $\sum_\kappa \exp(i\vec{G}\cdot\vec{r}_\kappa)$, where κ runs through the atoms which remain in equivalent positions.

Table I summarizes the results of the analysis.

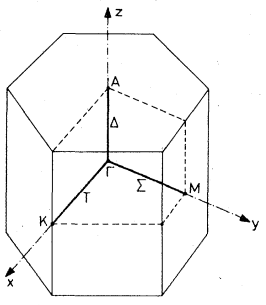

FIG. 4. Brillouin zone of Li_3N. Principal symmetry points and directions are shown. (see Table I).

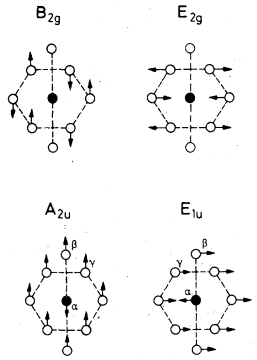

FIG. 5. Normal modes of vibration of Li_3N corresponding to different irreducible representations at the Γ point. (See Table II).

The allowed irreducible representations corresponding to special points or lines in the BZ are shown. The various compatibility relations between symmetry points and lines are also indicated.[12] The modes A and B are nondegenerate and the modes E are doubly degenerate. At the Γ point one of the three A_{2u} and one of the three E_{1u} modes belong to the acoustical branches. The remaining $2A_{2u}$ and $2E_{1u}$ modes are infrared active and are allowed for the electric vector E parallel and perpendicular to the z axis, respectively. The B_{2g} mode is both Raman and infrared inactive. The Raman-active E_{2g} mode is allowed for (xx), (yy), and (xy) configurations.[12] These predictions are consistent with the experimental observation (see Figs. 2 and 3, and Fig. 3 of Ref. 9), thus enabling the symmetry assignments to the observed modes.

The symmetry eigenvectors of normal modes at different points in the BZ were constructed using the projection operator technique.[10,11] Figure 5 depicts the motion of the ions for the different modes at the Γ point. The displacements of ions are parallel to the z axis for the B_{2g} and A_{2u} modes whereas they are perpendicular to the z axis for the E_{2g} and E_{1u} modes. The symbols α, β, and γ refer to the displacement amplitudes of the re-

TABLE I. Symmetries, irreducible representations and the compatibility relations of various symmetry points in the Brillouin zone of Li_3N.

Point	q (0<ζ<1)	G_q	Allowable irreducible representations and compatibility relations			
Γ	(0, 0, 0)	D_{6h}	$3A_{2u}$	$1B_{2g}$	$3E_{1u}$	$1E_{2g}$
Δ	$\frac{\Pi}{c}(0, 0, \zeta)$	C_{6v}	$3A_1$	$1B_1$	$3E_1$	$1E_2$
A	$\frac{\Pi}{c}(0, 0, 1)$	D_{6h}	$1A_{1g}$ $2A_{2u}$	$1B_{2g}$	$1E_{1g}$ $2E_{1u}$	$1E_{2g}$
K	$\frac{4\Pi}{3a}(1, 0, 0)$	D_{3h}	$2A_2'$	$1E''$	$1A_2'$ $3E'$	$1A_1'$
T	$\frac{4\Pi}{3a}(\zeta, 0, 0)$	C_{2v}	$3B_2$	$1A_2$	$4B_1$	$4A_1$
Γ	(0, 0, 0)	D_{6h}	$3A_{2u}$	$1B_{2g}$	$3E_{1u}$	$1E_{2g}$
Σ	$\frac{2\Pi}{\sqrt{3}a}(0, \zeta, 0)$	C_{2v}	$4B_2$		$4A_1$	$4B_1$
M	$\frac{2\Pi}{\sqrt{3}a}(0, 1, 0)$	D_{2h}	$3B_{1u}$	$1B_{2g}$	$3B_{3u}$ $1A_{1g}$	$3B_{2u}$ $1B_{1g}$

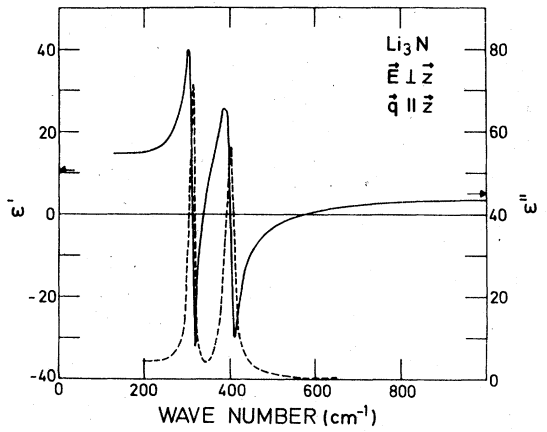

FIG. 6. Real and imaginary parts ϵ' (solid curve) and ϵ'' (dashed curve) of the complex dielectric function $\hat{\epsilon}$ of Li_3N obtained from a Kramers-Kronig analysis of the reflectivity data for $\vec{E} \perp \vec{z}$.

spective ions. The eigenvectors at the principal symmetry points and lines are summarized in Table II. It is interesting to note that the displacements of ions for the modes at Γ, Δ, A, Σ, and M points are polarized along one of the three Cartesian axes. On the other hand the displacements of lithium ions in the hexagonal plane are polarized along both x and y axes for K and T.

B. Kramers-Kronig analysis

Assuming a constant value of reflectivity below and above the measured range of frequencies, a Kramers-Kronig integration was performed to obtain the phase angle of the complex reflectivity. The optical constants were then calculated from Fresnel's formula. Figures 6 and 7 show the real part ϵ' and the imaginary part ϵ'' of the complex dielectric function $\hat{\epsilon}$ obtained from the Kramers-Kronig analysis of the reflectivity data of Figs. 2 and 3. The TO- and LO-phonon frequencies occur at the maxima of the ϵ'' spectra and at the above-resonance (positive-slope) zero crossings of the ϵ' spectra, respectively. Table III contains the TO and LO frequencies and the static and high-frequency dielectric constants, ϵ_0 and ϵ_∞, for $E \perp z$ and $E \parallel z$. The values of ϵ_∞ are from the measured values of reflectivity at 4000 cm^{-1}.

C. Oscillator fits

An oscillator model with the following expression for $\hat{\epsilon}$ was used to fit the reflectivity data:

$$\hat{\epsilon}(\omega) = \epsilon'(\omega) + i\epsilon''(\omega) = \epsilon_\infty + \sum_{j=1}^{2} \frac{S_j^2}{\omega_j^2 - \omega^2 - i\gamma_j\omega} . \quad (3)$$

Here S_j, ω_j, and γ_j are the strength, position, and damping of the jth oscillator, respectively. The parameters were chosen manually with the aid of a minicomputer equipped with a plotter. The calculated reflectivity curves were overlaid on the experimental data for comparison. This procedure was continued till the best fit was obtained.

The solid curve in Fig. 8 shows the results of such a fit. The open circles are the experimental points. It can be seen that the fit is not good at low frequencies. Attempts to fit that portion always resulted in a overall deterioration of the fit. The weak structure on top of the second oscillator for $\vec{E} \perp \vec{z}$ was observed for $\vec{q} \parallel \vec{z}$ measurements only (see Figs. 1 and 2) and is perhaps due to frequency-dependent damping arising from second-order processes. The fitted values of frequencies and dielectric constants are in good agreement with the values of Table III. The ϵ_0 values were given by

$$\epsilon_0 = \epsilon_\infty + \sum_{j=1}^{2} \frac{S_j^2}{\omega_j^2} . \quad (4)$$

The components of the effective charge tensor[13] for the nitrogen ion evaluated from the infrared data are $-1.8e$ and $-2.6e$, parallel and perpendicular to the z axis, respectively. This suggests that the nitrogen ion is in a N^{3-} state with a strong dynamic screening in the direction of the z axis (see Ref. 9 for details).

D. Lattice-dynamical model

We consider the short-range interactions between the neighboring ions indicated by springs in Fig. 1 and begin with the determination of the symmetries of the force-constant matrices.[14] We shall denote the longitudinal components of the forces by the symbol A and the transverse components by B if parallel to the hexagonal plane and by C otherwise. The matrices corresponding to the pairs of ions which are connected in or parallel to the yz plane (see Fig. 1) are then

$$\Phi(1,2) = -\frac{e^2}{2v} \begin{pmatrix} B_{12} & 0 & 0 \\ 0 & B_{12} & 0 \\ 0 & 0 & A_{12} \end{pmatrix}, \quad (5)$$

$$\Phi(1,3) = \Phi(1,4) = -\frac{e^2}{2v} \begin{pmatrix} B_{13} & 0 & 0 \\ 0 & A_{13} & 0 \\ 0 & 0 & C_{13} \end{pmatrix}, \quad (6)$$

$$\Phi(3,4) = -\frac{e^2}{2v} \begin{pmatrix} B_{34} & 0 & 0 \\ 0 & A_{34} & 0 \\ 0 & 0 & C_{34} \end{pmatrix}, \quad (7)$$

and

TABLE II. Symmetry eigenvectors corresponding to irreducible representations of various symmetry points in the BZ of Li_3N.

Point	Irreducible representation	Eigenvector N(1)			Li(2)			Li(3)			Li(4)		
Γ	E_{1u}	α	0	0	β	0	0	γ	0	0	γ	0	0
		0	α	0	β	0	0	γ	0	0	0	γ	0
	A_{2u}	0	0	α	0	0	β	0	0	γ	0	0	γ
	E_{2g}	0	0	0	0	0	0	$1/\sqrt{2}$	0	0	$-1/\sqrt{2}$	0	0
		0	0	0	0	0	0	0	$1/\sqrt{2}$	0	0	$-1/\sqrt{2}$	0
	B_{2g}	0	0	0	0	0	0	0	0	$1/\sqrt{2}$	0	0	$-1/\sqrt{2}$
Δ	E_1	α	0	0	0	β	0	γ	0	0	γ	0	0
		0	α	0	0	β	0	0	γ	0	0	γ	0
	A_1	0	0	α	0	0	β	0	0	γ	0	0	γ
	E_2	0	0	0	0	0	0	$1/\sqrt{2}$	0	0	$-1/\sqrt{2}$	0	0
		0	0	0	0	0	0	0	$1/\sqrt{2}$	0	0	$-1/\sqrt{2}$	0
	B_1	0	0	0	0	0	0	0	0	$1/\sqrt{2}$	0	0	$-1\sqrt{2}$
A	E_{1u}	α	0	0	0	0	0	β	0	0	β	0	0
		0	α	0	0	0	0	0	β	0	0	β	0
	A_{2u}	0	0	α	0	0	0	0	0	β	0	0	β
	E_{1g}	0	0	0	1	0	0	0	0	0	0	0	0
		0	0	0	0	1	0	0	0	0	0	0	0
	A_{1g}	0	0	0	0	0	1	0	0	0	0	0	0
	E_{2g}	0	0	0	0	0	0	$1/\sqrt{2}$	0	0	$-1/\sqrt{2}$	0	0
		0	0	0	0	0	0	0	$1/\sqrt{2}$	0	0	$-1/\sqrt{2}$	0
	B_{2g}	0	0	0	0	0	0	0	0	$1/\sqrt{2}$	0	0	$-1/\sqrt{2}$
Σ	B_1	α	0	0	β	0	0	γ	0	0	δ	0	0
	A_1	0	α	0	0	β	0	0	γ	0	0	δ	0
	B_2	0	0	α	0	0	β	0	0	γ	0	0	δ
M	B_{2u}	α	0	0	β	0	0	γe^{-i60°	0	0	γe^{i60°	0	0
	B_{3u}	0	α	0	0	β	0	0	γe^{-i60°	0	0	γe^{i60°	0
	B_{1u}	0	0	α	0	0	β	0	0	γe^{-i60°	0	0	γe^{i60°
	B_{1g}	0	0	0	0	0	0	$(1/\sqrt{2})e^{i30^\circ}$	0	0	$(1\sqrt{2})e^{-i30^\circ}$	0	0
	A_{1g}	0	0	0	0	0	0	0	$(1/\sqrt{2})e^{i30^\circ}$	0	0	$(1\sqrt{2})e^{-i30^\circ}$	0
	B_{2g}	0	0	0	0	0	0	0	0	$(1\sqrt{2})e^{i30^\circ}$	0	0	$(1/\sqrt{2})e^{-i30^\circ}$
T	A_1	α	0	0	β	0	0	γ	$i\delta$	0	γ	$-i\delta$	0
	B_1	0	α	0	0	β	0	$i\gamma$	δ	0	$-i\gamma$	δ	0
	B_2	0	0	α	0	0	β	0	0	γ	0	0	γ
	A_2	0	0	0	0	0	0	0	0	$1/\sqrt{2}$	0	0	$-1/\sqrt{2}$
K	E'	α	0	0	β	0	0	γ	$i\gamma$	0	γ	$-i\gamma$	0
		0	α	0	0	β	0	$i\gamma$	γ	0	$-i\gamma$	γ	0
	A_2''	0	0	α	0	0	β	0	0	0	0	0	0

TABLE II. (*Continued*)

Point	Irreducible representation	N(1)	Li(2)	Eigenvector Li(3)		Li(4)	
	A_1'	0	0	$-\frac{1}{2}i$	0	$\frac{1}{2}i$	0
	A_2'	0	0	$\frac{1}{2}$	0	$\frac{1}{2}$	0
	E''	0	0	0	$1/\sqrt{2}$	0	$1/\sqrt{2}$
		0	0	0	$1/\sqrt{2}$	0	$-1/\sqrt{2}$
		0	0	$\frac{1}{2}$	0	$-\frac{1}{2}i$	0
		0	0	$-\frac{1}{2}i$	0	$\frac{1}{2}$	0

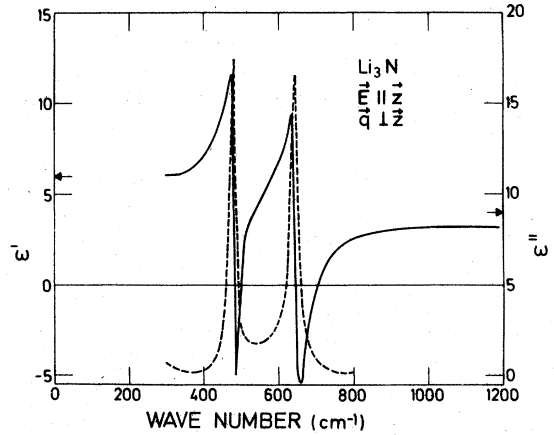

FIG. 7. ϵ' (solid curve) and ϵ'' (dashed curve) of Li_3N for $\vec{E} \| \hat{z}$ obtained from a Kramers-Kronig analysis.

$$\Phi(2,4) = -\frac{e^2}{2v}\begin{pmatrix} B_{24} & 0 & 0 \\ 0 & 4\dfrac{(A_{24}-C_{24})}{4+h^2}+C_{24} & -2h(A_{24}-C_{24}) \\ 0 & -2h(A_{24}-C_{24}) & h^2\dfrac{(A_{24}-C_{24})}{4+h^2}+C_{24} \end{pmatrix} \tag{8}$$

Here e and v are the electronic charge and the volume of the unit cell, respectively. In Eq. (8), $h = \sqrt{3}c/a$. The matrices for other equivalent pairs of ions are related to the corresponding ones given here by rotations along the z axis.

We neglect the polarizability of lithium ions and consider the nitrogen ions to be anisotropically polarizable. This polarizability is described by a shell with a charge Y and coupled to the core by a tensor of the form

$$G(1) = \begin{bmatrix} G_\perp & 0 & 0 \\ 0 & G_\perp & 0 \\ 0 & 0 & G_\parallel \end{bmatrix}. \tag{9}$$

The dynamical matrix for the shell model[15] is written as

$$D = M^{-1/2}\{R + ZCZ - (R + ZCY) \times (R + G + YCY^{-1})(R + ZCY)^{\dagger}\}M^{-1/2}. \tag{10}$$

In the above equation R is the 12×12 matrix for the short-range interactions which is obtained by the Fourier transforms of the matrices Φ. The expressions are given in the Appendix. The Li-N interactions are via the lithium ion and the nitrogen shell. The diagonal tensors M and Z contain the atomic masses and the static ionic charges of

TABLE III. Phonon frequencies (in cm^{-1}) and dielectric constants for Li_3N as determined from a Kramers-Kronig analysis of the infrared reflectivity data.

	$\vec{E} \perp \vec{z}$	$\vec{E} \parallel \vec{z}$
TO_1	316 ± 4	481 ± 4
LO_1	338 ± 2	503 ± 4
TO_2	404 ± 5	645 ± 4
LO_2	575 ± 2	708 ± 2
ϵ_0	10.5 ± 1.5	6.0 ± 2.0
ϵ_∞	5.0 ± 0.5	4.0 ± 0.5

N and Li. The latter are taken to be $-3e$ and $+1e$, respectively, for the following reasons: first of all, the x-ray analysis supports static charges with these values[16]; secondly, our infrared analysis gave a transverse effective charge $-2.6e$ for N which is close to $-3e$. Furthermore, the scaling of the Coulomb forces between Li^+ and N^{3-} as compared to those in Li^+F^- suggests an enhancement of these forces by a factor of about 3, corresponding to the charge $-3e$ of N^{3-} as compared to $-1e$ of F^- (see below). The tensors Y and G contain the shell charge and the shell-core interaction of the nitrogen, respectively. The matrix of the Fourier transforms of the Coulomb interactions is denoted by C.

The nine experimental frequencies of zone-center optical phonons (four pairs of infrared active LO and TO and the Raman-active modes) were used to determine the parameters of the model. Due to the simple expressions of the dynamical matrix at the zone center, the fits could be obtained without the aid of a computer. In the most general case with all the above described interactions there would be 14 parameters, not counting the ionic charges which remain fixed. A preliminary calculation was performed with a Born-Mayer potential[17] using only one set of parameters for all the Li-Li interactions and another for all Li-N interactions. This calculation indicated that the Li-Li interactions are very weak in comparison with the Li-N interactions. In the second step the Li-Li forces were ignored and the N-Li forces were considered noncentral but axially symmetric, i.e. $B_{13} = C_{13}$. In this model a good fit for the experiment was obtained with only seven parameters.

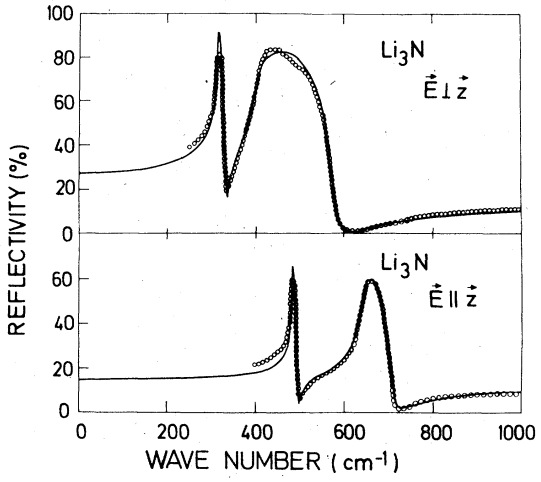

FIG. 8. Oscillator fits (solid curves) to the experimental reflectivity spectra (open circles).

However, some acoustical modes were unstable at the M and K points. Any attempt to remove this instability resulted in the deterioration of the fit. Stable solutions for the dispersion curves and a good fit to the experiment could be obtained only by assuming a strong axial asymmetry for the N-Li interaction in the hexagonal plane. The best-fit values of the eight parameters used in the model are shown in Table IV. It is interesting to note that the parameters for the N-Li forces are about three times larger than those for the corresponding interactions in lithium halides.[18] These large repulsive forces are required to compensate the attractive Coulomb forces which are three times larger in Li_3N than in the lithium halides due to the charge -3 of the nitrogen ion instead of -1 of the anions in the halides.

E. Analysis of the dispersion relations

Figure 9 depicts the calculated dispersion relation. The experimental data at the Γ point are also shown for comparison. It should be mentioned that the fit is very good. The maximum deviation from the experimental data is about 5%, which occurs for the highest TO frequency of A_{2u} symmetry. The following observations about the

TABLE IV. Best-fit shell-model parameters. The symbols || and ⊥ refer to the z axis.

	N – Li					N		
Units			$e^2/2v$			e	e^2/v	
Parameters	A_{12}	B_{12}	A_{13}	B_{13}	C_{13}	Y	$G_{\parallel}$	$G_{\perp}$
Value	90.0	−16.8	76.5	−26.5	−2.0	−3.75	50.8	45.7

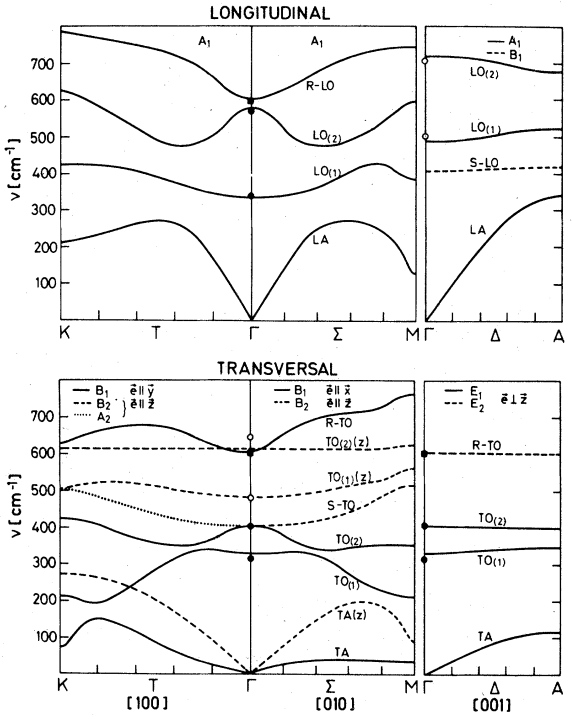

FIG. 9. Dispersion curves of Li_3N. The experimental data of the ir- and Raman-active modes at the Γ point are indicated by the symbols: ● E_{1u}, ○ A_{2u}, and ■ E_{2g}. The transverse (T) and longitudinal (L) branches are numbered according to the corresponding modes at the Γ point as in Table III. The modes polarized along the z axis are indicated by (z). The letters s and R prior to the symbol designating the phonon branch refer to the silent mode and the Raman-active mode at the Γ point, respectively. The silent mode (B_{2g}) is accidentally degenerate with the A_{2u} mode at 404 cm^{-1}.

dispersion relations can be made: There are low-lying acoustical modes and some of them tend to become unstable at the zone boundary in the (xy) plane. Also the dispersion surfaces in this plane are nearly isotropic as indicated by the curves along the T and Σ directions in Fig. 9. In contrast to the shape of the dispersion curves in these directions, that along the Δ direction is generally flat. Unfortunately the neutron scattering data are not yet available and hence no verification of the dispersion curves can be made. However, the structures in the second-order Raman spectra can be tentatively explained on the basis of our calculations.

The Raman spectrum of Li_3N for $x(zz)\bar{x}$ is shown in Fig. 10. In this configuration the first-order line is not allowed. The spectrum shown is due to two-phonon processes only, except for a small polarization leakage of the first-order line at 600 cm^{-1}. It is well known that the second-order Raman spectra are characteristic of the density of states and the matrix elements of the polarizability tensor. The sharp features can be explained by the overtones or combinations of phonons at the symmetry points in the Brillouin zone. The observed spectra have a cutoff at ~1500 cm^{-1} which corresponds to the overtones of the highest optical branches. In Fig. 10 we propose an assignment consistent with the dispersion relations shown in Fig. 9. It appears that the overtones of phonons propagating in the Δ direction contribute strongly to the spectra. This is understandable due to the flatness of these branches which leads to high density of states.

It has been shown[5] that the second-order Raman scattering in oxides arises mainly from the intraionic polarizability of the O^{2-} ion. In alkali-earth oxides this ion is the lightest one, and hence the main contribution originates from the high-lying optical branches. In an analogous manner, the intraionic polarizability of the N^{3-}, which is the heavier of the ions in Li_3N, should contribute to the second-order spectra in the region of the overtones of the acoustical branches. Indeed the

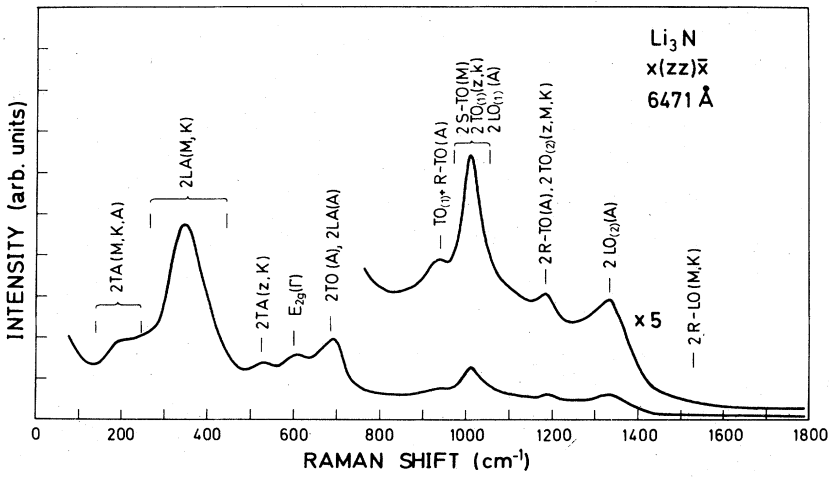

FIG. 10. Second-order Raman spectrum of Li_3N for $x(zz)\bar{x}$. The 6471-Å line of a Kr^+ laser was used to excite the spectrum. A symmetry assignment of the structures in the spectrum is made according to Fig. 9.

strongest part of the observed spectra in Fig. 10 corresponds to the overtones of the TA and LA branches of the dispersion curves in Fig. 9. A calculation of the second-order Raman cross section including the intraionic polarizability of the N^{3-} ion is in progress.[6]

F. Calculation of the dielectric properties

The well-known expression of the high-frequency dielectric constant for the shell model[19] in the present case, where the only contribution comes from nitrogen, reduces to

$$\epsilon_{\infty\perp} = 1 + 4\pi[(\alpha_\perp/v)/(1 - 4.938\alpha_\perp/v)] , \tag{11}$$

and

$$\epsilon_{\infty\parallel} = 1 + 4\pi[(\alpha_\parallel/v)/(1 - 2.690\alpha_\parallel/v)] . \tag{12}$$

Here $\alpha_\perp$ and $\alpha_\parallel$ are the components of the nitrogen polarizability perpendicular and parallel to the hexagonal axis, respectively, which are given by

$$\alpha_\perp = Y^2/[G_\perp + B_{12} + \tfrac{3}{2}(A_{13} + B_{13})] \tag{13}$$

and

$$\alpha_\parallel = Y^2/(G_\parallel + A_{12} + 3C_{13}) . \tag{14}$$

The values of parameters in Table IV lead to $\alpha_\perp = 6.04$ Å^3 and $\alpha_\parallel = 4.66$ Å^3. These values are even higher than those found for the O^{2-} ion, which vary between 0.4 and 3.0 Å^3.[20] This suggests that the valence electrons of the N^{3-} ion are very loosely bound, as is to be expected if this ion is stable only because of its crystal environment. According to Eqs. (11) and (12) the high-frequency dielectric constants have the values $\epsilon_{\infty\perp} = 6.1$ and $\epsilon_{\infty\parallel} = 2.8$, in good agreement with the experimental values given in Table III. From the generalized form of the Lyddane-Sachs-Teller relation[13] we obtain the values $\epsilon_{0\perp} = 12.4$ and $\epsilon_{0\parallel} = 3.9$ for the static dielectric constants, which again compare well with the experimental values of Table III.

IV. CONCLUSIONS

The lattice-dynamical properties of Li_3N have been investigated both theoretically and experimentally. The infrared and Raman data can be explained satisfactorily in terms of a shell model, with eight parameters, which contains nearest-neighbor interactions only and includes an anisotropic polarizability of the nitrogen ion. The dynamic charge of the nitrogen ion is obtained from the infrared data and its static charge involved in the lattice-dynamical model lead to the conclusion that in this material the nitrogen ions are close to an anomalous N^{3-} state. This is the first known evidence for the N^{3-} state in a nitrogen compound. The large and anisotropic polarizability of the nitrogen, which is related to a highly deformable filled ($2p^6$) shell, might support the high mobility of the lithium ions in Li_3N. As in oxides such as MgO, the predominant part of the second-order Raman spectrum seems to originate from the intraionic polarizability of the N^{3-} ion which is highly unstable as a free ion. Detailed investigations of this aspect are in progress.

ACKNOWLEDGMENTS

We thank G. Müller for the preparation of the crystals, A. Breitschwerdt, G. Fröhlich, and W. König for technical assistance, and T. P. Martin for the critical reading of the manuscript. Many discussions with M. Chandrasekhar, A. Rabenau, and H. Wendel are gratefully acknowledged.

APPENDIX: THE SHORT-RANGE MATRIX R

The complete 12×12 matrix R for the short-range forces can be split up into the (3×3) matrices $R(\vec{q}, \kappa\kappa')$ for each pair of particles $(\kappa\kappa')$, which satisfy the following relations:

$$R(\vec{q}, \kappa\kappa') = R^T(\vec{q}, \kappa\kappa') = R(-\vec{q}, \kappa'\kappa) . \tag{A1}$$

For $(\kappa\kappa') = (1\,3)$, $(4\,1)$, $(3\,4)$, $(2\,3)$, or $(4\,2)$ the corresponding matrices can be summarized, in units of e^2/v, by

$$\begin{pmatrix} -\{\frac{1}{2}BE_y^{-2} + [3P + \frac{1}{4}(B+3C)]C_xE_y\}C_z & -i\sqrt{3}[P + \frac{1}{4}(C-B)]S_xE_yC_z & \sqrt{3}hPS_xE_yS_z \\ & -\{\frac{1}{2}(4P+C)E_y^{-2} + [P + \frac{1}{4}(3B+C)]C_xE_y\}C_z & ihP(E_y^{-2} - C_xE_y)S_z \\ & & -(h^2P + C)(\frac{1}{2}E_y^{-2} + C_xE_y)C_z \end{pmatrix} , \tag{A2}$$

where only the upper half of the matrix is given, since it is symmetric. Here we define:

$$P = (A - C)/(4 + h^2) , \tag{A3}$$

$$h = \sqrt{3}c/a , \tag{A4}$$

$$E_y = \exp[\tfrac{1}{2}(iq_ya/\sqrt{3})] , \tag{A5}$$

$$C_x = \cos\tfrac{1}{2}q_xa , \tag{A6}$$

$$C_z = \cos\tfrac{1}{2}q_zc , \tag{A7}$$

and S_x, S_z are the analogous sines. For the cases $(\kappa\kappa') = (1\,3), (4\,1), (3\,4)$, it is taken $c = 0$.

The correspondence between A, B, C, and the force constants introduced in Sec. IIID is given in each case by

$$(\kappa\kappa') \quad A \quad B \quad C \,,$$

$$(1\,3) \qquad A_{13} \quad B_{13} \quad C_{13} \,,$$

$$(4\,1) \qquad A_{34} \quad B_{34} \quad C_{34} \,,$$

$$(3\,4) \qquad 2A_{24} \quad 2B_{24} \quad 2C_{24} \,.$$

$$(2\,3) \qquad$$

$$(4\,2)$$

The matrix corresponding to the pairs of atoms (1 2) is expressed in units of e^2/v as follows:

$$R(\vec{q}, 12) = \begin{pmatrix} -B_{12}C_z & 0 & 0 \\ 0 & -B_{12}C_z & 0 \\ 0 & 0 & -A_{12}C_z \end{pmatrix}. \tag{A8}$$

The matrices $R(\vec{q}, \kappa\kappa)$ are obtained from the translation invariance relations:

$$R(\vec{q}, \kappa\kappa) = -\sum_{\kappa'(\kappa' \neq \kappa)} R(0, \kappa\kappa') \,. \tag{A9}$$

---

*Present address: Department of Physics, University of Missouri at Columbia, Columbia, Mo. 65201.

[1]B. A. Boukamp and R. A. Huggins, Phys. Lett. A 58, 231 (1976).

[2]U. V. Alpen, A. Rabenau, and G. H. Talat, Appl. Phys. Lett. 30, 621 (1977).

[3]G. C. Farrington and W. L. Roth, in *Superionic Conductors*, edited by G. D. Mahan and W. L. Roth (Plenum, New York, 1976), p. 418.

[4]M. S. Wittingham and R. A. Huggins, in *Solid State Chemistry*, edited by R. S. Roth and J. S. Schneider, Natl. Bur. Stds. Spec. Publ. No. 364 (U.S. GPO, Washington, D.C., 1972), p. 139.

[5]See, for example, M. Buchanan, R. Haberkorn, and H. Bilz, J. Phys. C 7, 439 (1974); R. Migoni, H. Bilz, and D. Bäuerle, Phys. Rev. Lett. 37, 1155 (1976).

[6]H. R. Chandrasekhar, R. Migoni, and H. Bilz (unpublished).

[7]E. Zintl and G. Brauer, Z. Elektrochem. 41, 102 (1935).

[8]A. Rabenau and H. Schulz, J. Less Common Metals 50, 155 (1976); for crystal growth see G. Müller and E. Schönherr, J. Cryst. Growth (to be published).

[9]H. R. Chandrasekhar, G. Bhattacharya, R. Migoni, and H. Bilz, Solid State Commun. 22, 681 (1977).

[10]A. A. Maradudin and S. H. Vosko, Rev. Mod. Phys. 40, 1 (1968).

[11]S. H. Chen, Phys. Rev. 163, 532 (1967).

[12]See, for example, E. B. Wilson, J. C. Decius, and P. C. Cross, *Molecular Vibrations* (McGraw-Hill, New York, 1955).

[13]T. Kurosawa, J. Phys. Soc. Jpn. 16, 1298 (1961).

[14]A. A. Maradudin, E. W. Montroll, G. H. Weiss, and I. P. Ipatova, in *Solid State Physics* (Academic, New York, 1971), Suppl. 3.

[15]W. Cochran, Crit. Rev. Solid State Sci. 2, 1 (1971).

[16]A. Rabenau and H. Schulz (unpublished).

[17]M. Born and K. Huang, *Dynamical Theory of Crystal Lattices* (Oxford University, Oxford, 1954).

[18]C. R. A. Catlow, K. M. Diller, and M. J. Norgett, J. Phys. C (to be published).

[19]R. A. Cowley, Proc. R. Soc. A 268, 121 (1962).

[20]R. Kirsch, A. Gérard, and M. Wautelet, J. Phys. C 7, 3633 (1974).